J Sol-Gel Sci Technol (2013) 68:136–140
DOI 10.1007/s10971-013-3145-z

ORIGINAL PAPER

Magnetoelectric $Bi_{3.25}Nd_{0.75}Ti_3O_{12}$–$La_{0.6}Ca_{0.4}MnO_3$ composite thin films derived by SOL–GEL method

C. P. Cheng · Z. H. Tang · M. H. Tang · Y. C. Zhou

Received: 10 May 2013 / Accepted: 19 August 2013 / Published online: 24 August 2013

Abstract Magnetoelectric (ME) $Bi_{3.25}Nd_{0.75}Ti_3O_{12}$–$La_{0.6}Ca_{0.4}MnO_3$ (BNT–LCMO) composite thin films were deposited on Pt/Ti/SiO_2/Si(100) substrates by a simple SOL–GEL method and spin-coating process with two different deposition sequences: BNT/LCMO/Pt/Ti/SiO_2/Si(BLP) and LCMO/BNT/Pt/Ti/SiO_2/Si(LBP). Our results show the composite thin films exhibit both good ferroelectric and magnetic properties, as well as a ME effect. BLP thin films have larger maximum ME voltage coefficient values than LBP structured thin films. The deposition sequence has a notable effect on the ferroelectric and magnetic properties and ME coupling behavior of the bilayer thin films.

Keywords Deposition sequence · Ferroelectric · Magnetic · Magnetoelectric

1 Introduction

Multiferroics, which have electric, magnetic, and structural order parameters in the same phase, have attracted tremendous fundamental and practical interest for their simultaneous ferroelectricity, ferromagnetism, and ferroelasticity [1–4]. As is known to all, magnetoelectric (ME) effect is a cross two-field effect, characterized by appearance of an electric polarization P upon applying a magnetic field H or with the change of magnetization M on applying an electric field E [5–7]. Besides the ferroelectromagnets as the longtime objects of the related researches, ME-composite materials represent the systems where strong ME effect is predicted based on the idea of product property of composite materials [8]. A lot of research work has indicated that developing composite multiferroics by artificially making ferroelectrics and ferromagnets into nanoscale heterostructures may be an effective technique for obtaining the large ME effect [9–19]. In constructing the layered ME composite film structures, there are many parameters to be optimized, in which the growth sequence of these two phases on the substrate should result in an influence on the properties of the resultant composite films [20]. Based on the above, perovskite $Bi_{3.25}Nd_{0.75}Ti_3O_{12}$(BNT) and $La_{0.6}Ca_{0.4}MnO_3$(LCMO) are selected as the ferroelectric and ferromagnetic phases in the present composite thin films respectively and, the effects of deposition sequence on the electrical properties and the ME coupling behaviors of the BNT–LCMO composite thin films are investigated.

2 Experimental details

We have succeeded in synthesizing BNT–LCMO composite films with both ferroelectric and ferromagnetic properties, as well as ME effect at room temperature. In this article, we report effects of deposition sequence on the properties of BNT–LCMO composite thin films derived by SOL–GEL method. ME BNT–LCMO composite thin films were deposited on Pt/Ti/SiO_2/Si(100) substrates by SOL–GEL method with two different deposition sequences: BNT/LCMO/Pt/Ti/SiO_2/Si(BLP) and LCMO/BNT/Pt/Ti/SiO_2/Si(LBP). To

C. P. Cheng (✉) · Z. H. Tang · M. H. Tang (✉) · Y. C. Zhou
Key Laboratory of Low Dimensional Materials and Application Technology of Ministry of Education, Xiangtan University, Xiangtan 411105, Hunan, China
e-mail: chengchuanpin@163.com

M. H. Tang
e-mail: mhtang@xtu.edu.cn

C. P. Cheng
Faculty of Science, Hunan Institute of Engineering, Xiangtan 411104, Hunan, China

obtain the precursor solution of BNT, bismuth nitrate [$Bi(NO_3)_3{\cdot}5H_2O$], neodymium nitride [$Nd(NO_3)_3$], and titanium butoxide [$Ti(OC_4H_9)_4$] were used as starting materials for Bi, Nd and Ti, respectively. Separately, in a beaker, Bismuth nitrate (10 mol% excess) and neodymium nitride were dissolved at 40 °C in glacial acetic acid [CH_3COOH], titanium butoxide was dissolved in glacial acetic acid, and acetylacetone [CH_3COCH_2–$COCH_3$] was used as the chelating agent. The titanium solution was added to the bismuth-dysprosium solution with continuous stirring, and the final mixture was stirred for an additional 30 min. Then, acetylacetone was added to the solution as a stabilizing agent. Finally, 2-methoxyethanol was added to adjust the concentration. A clear purple sol was obtained. A 10 mol % excess amount of bismuth nitride was used to compensate for the Bi evaporation during annealing. To obtain the precursor solution of LCMO, lanthanum acetate, calcium acetate and manganese acetate were dissolved in an aqueous solution of citric acid with the metal atomic ratio La/Ca/Mn of 0.4:0.6:1. After the chelating reaction, polyethylene glycol as a kind of surfactant and ethanol were added into LCMO solution. The final concentration of two kinds of precursor solutions was approximately 0.1 M. The preparation of the films consisted in spin coating the Pt(111)/Ti/SiO2/Si(100) substrates with the stock solution at 3,000 rpm for 30 s. The wet film samples were then fully dried in a rapid thermal processor (RTP-500) at 180 °C for 3 min followed by another 3 min at 400 °C to remove residual organic compounds. This coating process is referred to as one deposition. The coating and preheating process should be repeated several times to obtain the desired film thickness. Both BNT and LCMO layers were fabricated using six depositions. Post annealing was performed at 750 °C for 15 min under an oxygen atmosphere by a rapid thermal annealing process. The final composite thin films were formed with a thickness of ~1 μm (see Fig. 2c), accompanying with the deep diffusion between the LCMO layers and BNT layers. The crystal structure was characterized by X-ray diffraction (XRD). The microstructures of the films were examined by scanning electron microscopy (SEM). For electrical measurements, Au top electrodes with a diameter of 200 μm were coated on the composite thin films by DC sputtering using a shadow mask. The ferroelectric and leakage current measurements were performed using a Radiant Technologies Precision Workstation ferroelectric test system. Magnetic properties and ME effects of the films were measured using a vibrating sample magnetometer and a ME measuring system at room temperature, respectively.

3 Results and discussion

Figure 1 shows the typical XRD patterns of BLP and LBP composite thin films. All the diffraction peaks were identified and indexed according to the standard powder diffraction data of BNT and LCMO. Two evident sets of well defined peaks are observed in the thin films, which belong to polycrystalline bismuth-layered perovskite structure BNT and LCMO. There are no additional or intermediate phase peaks apart from BNT and LCMO, which confirming the preparation of a material containing both ferromagnetic and ferroelectric phases. For the chemical interaction between the ferroelectric and ferromagnetic phases would lead to their ferroelectric or magnetic properties degrading, it is very important that no additional or intermediate phase exist for the preparation of ferroelectric-ferromagnetic composites [21].

Figure 2 displays the SEM surface morphologies of (a) BLP and (b) LBP composite thin films, and (c) the cross section of BLP composite thin films. From Fig. 2a, b, one can see that smooth surface and better crystallization degree of the composite thin films were obtained on Pt/Ti/SiO_2/Si substrates. The surface of the BLP film with the BNT as the top layer is more compact and smoother than that of LBP film, and the crystal particle size of BNT is smaller than LCMO, which implies that BNT layer is more compact than LCMO layer. So the electrical properties will be sensitively influenced by the deposition sequence of the different layered structures, which will be discussed later. From Fig. 2c, one can see that the final composite thin films were formed with a total thickness of ~1 μm, in which BNT and LCMO are both about 500 nm in thickness, accompanying with the deep diffusion between the LCMO layers and BNT layers.

The DC leakage current characteristics for LCMO-BNT composite thin films with different deposition sequences, i.e., the BLP and LBP structured composite thin films are shown in Fig. 3. From Fig. 3 one can see that compared with the LBP film, the BLP film has a smaller leakage current density. This is consistent with the fact that the

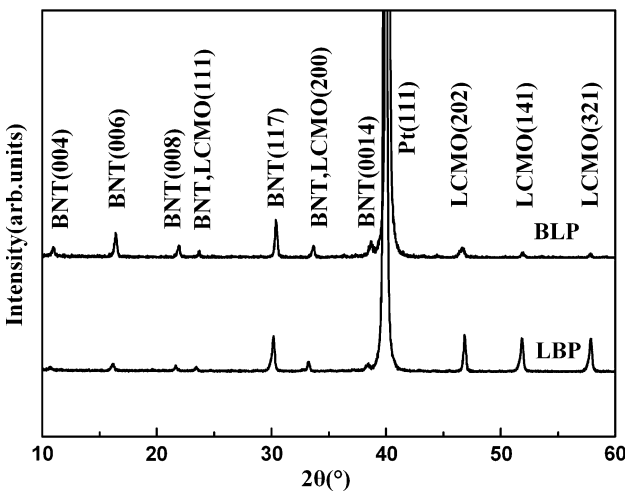

Fig. 1 XRD patterns of the composite thin films

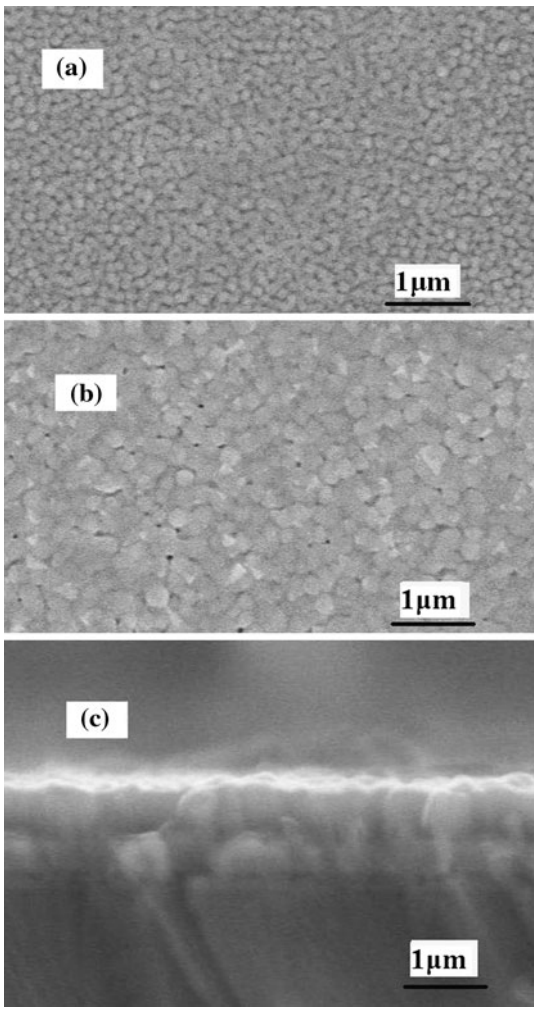

Fig. 2 SEM surface morphologies of **a** BLP and **b** LBP and **c** the cross section of BLP composite thin films

surface of the BLP film is more compact than that of the LBP film, which indicates that the insulating property of BLP is better than that of LBP.

Figure 4a displays the polarization versus electric field (*P-E*) hysteresis loops of BLP and LBP structured composite thin films. As shown in Fig. 4a, the well-defined ferroelectric loops are observed in the BLP and LBP films. The remnant polarization ($2P_r$) values of the deposited BLP and LBP composite thin films are 21.6 and 12.8 $\mu C/cm^2$, corresponding to the coercive fields of 84.9 and 76.5 kV/cm, respectively. Obviously, compared with the LBP film, the BLP film exhibits a higher P_r value, which is maybe owing to the better insulating property of the BLP film.

The magnetic hysteresis loops of BLP and LBP composite thin films are presented in Fig. 4b. As shown in Fig. 4b, magnetic hysteresis loops with saturation magnetization $M_s \sim 330$ emu/cm^3 of the BLP film and ~ 289 emu/cm^3 of the LBP film are observed, which hints the present thin films of an ordered magnetic structure. From Fig. 4b one can see that

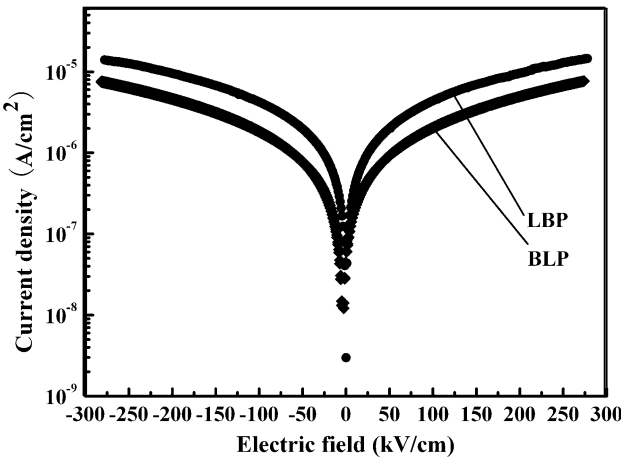

Fig. 3 The DC leakage current characteristics of the composite thin films

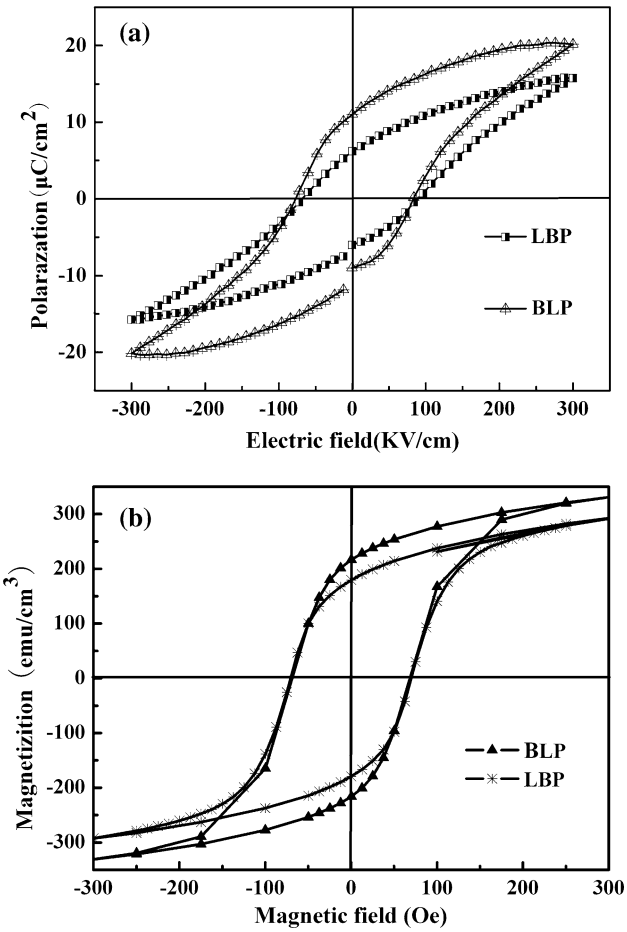

Fig. 4 **a** *P-E* hysteresis loops and **b** magnetic hysteresis loops of BLP and LBP structured composite thin films

the BLP film shows a larger saturation magnetization M_s value than the LBP film. This is consistent with the fact that the BLP film has a smaller leakage current density compared with the LBP film.

The coexistence of the ferroelectric BNT and ferromagnetic LCMO phases in the present composite thin films gives rise to a ME effect, which is characterized by the ME voltage coefficient $\alpha_E = dE/dH$. The ME effect is determined by the ME voltage coefficient α_E measured in terms of the induced electric field E under an applied AC magnetic field of H superimposed onto a DC bias magnetic field H_{bias}. The AC magnetic field H (10 Oe) generated by a pair of Helmholtz coils and a DC bias magnetic field H_{bias} generated by an electromagnet were superimposed and parallel to the film plane. The induced electric field E was measured using a lock-in amplifier (SRS Inc., SR830). Figure 5 shows the variations of ME voltage coefficient α_E as a function of applied magnetic bias H_{bias} at a fixed AC magnetic frequency $f = 1$ kHz for the BLP and LBP composite films, measured at room temperature. From Fig. 5 one can see that the composite films exhibit ME effect which is dependent on H_{bias}. As shown in Fig. 5, α_E values increase rather steeply with increasing H_{bias} that is below 110 Oe, when H_{bias} reaches 110 Oe, α_E reaches its largest values. However, it is noticeable that when H_{bias} reaches more than 110 Oe, the α_E value shows a rapid decline and then a gradual decrease to near zero with further increase of H_{bias}. This behavior may be explained by following discussions. Since the ME coupling in ME composites is arose from the AC field initiated dynamic Joule magnetostriction, caused by domain wall motion (at low fields close to coercivity) and rotation (at large fields far from coercivity), the magnetostrictive layer of high permeability, simultaneously showing large magnetostriction constant, would expect to produce a large ME effect [22]. This might explain the sharp increase of α_E in the low field. When the bias magnetic field reaches 110 Oe, α_E reaches its largest value, which has a larger magnitude than the coercivities. The maximum values of the α_E for the BLP and LBP structures are 69 and 63 mV/cm Oe, respectively. At higher bias fields, the magnetostriction of the LCMO layer gets saturated and producing a nearly constant electric field in the BNT ferroelectric phase and led to a slow reduction of α_E. In addition, it is obvious that α_E values of BLP film are larger than that of LBP film at any fixed H_{bias} in the range of 0–1,000 Oe, while they exhibit a similar rise-and-fall trend. This may be due to the enhancement of the interfacial coupling in the BLP film, characterized by the magnetic-mechanical-electric interaction between the magnetic and ferroelectric phases through the stress/strain in the interface [23], for top BNT layer in the BLP film has a more compact structure and less defects and better crystallization than LCMO, while the substrate layer has a smaller lattice mismatch with LCMO than with BNT.

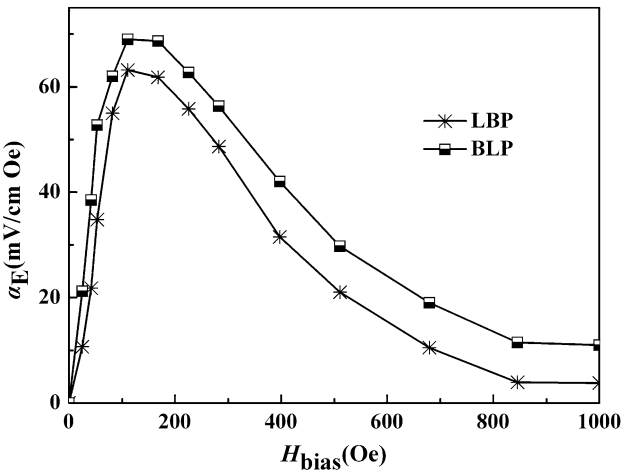

Fig. 5 Variation of α_E with H_{bias} at magnetic frequency $f = 1$ kHz for BLP and LBP composite thin films

4 Conclusion

In conclusion, the ME BNT–LCMO composite thin films were deposited on Pt/Ti/SiO_2/Si(100) substrates by SOL–GEL method and spin-coating process with two different deposition sequences: BLP and LBP. Our results show that the present two kinds of double-layered composite thin films exhibit both good ferroelectric and magnetic properties, as well as a ME effect at room temperature. Some differences in their ferroelectric and magnetic properties and ME coupling behavior are exhibited depending on their structures. The maximum ME voltage coefficient value of the BLP thin film is larger than the LBP structure. The composite thin films exhibit distinct ME coupling behaviors, while the ME voltage coefficient α_E of the BLP composite film is larger than that of the LBP composite film due to a possible enhancing of interface coupling. The BLP structured films have better ferroelectric properties and higher saturation magnetization than the LBP structured films. These results indicated that the deposition sequence has an obvious influence on the ferroelectric and magnetic properties and ME coupling behavior of the bilayer thin films.

Acknowledgments This work was supported by Key Project of National Natural Science Foundation of China (NSFC) (Grant No. 11032010), NSFC (Grant Nos. 51072171, 61274107, 61176093 and 11275163), PCSIRT (IRT1080), 973 Program (2012CB326404), Key Project of Scientific Research Fund of Hunan Provincial Education Department (12A129), Hunan Provincial Innovation Foundation for Postgraduate (CX2011B248), the Doctoral Program of Higher Education of China (Grant No. 20104301110001) and the Aid Program for Science and Technology Innovative Research Team in Higher Educational Institutions of Hunan Province.

References

1. Hill NA (2000) J Phys Chem B 104:6694
2. Cheong SW, Mostovoy M (2007) Nat Mater 6:13
3. Wang KF, Liu JM, Ren ZF (2009) Adv Phys 58:321
4. Choi T, Lee S, Choi YJ, Kiryukhin V, Cheong SW (2009) Science 63:324
5. Nan CW (1994) Phys Rev B 50:6082
6. Nan CW, Li M (2001) Appl Phys Lett 78:2527
7. Srinivasan G, Rasmussen ET, Levin BJ, Hayes R (2002) Phys Rev B 65:134402
8. Van Suchtelen J (1972) Philips Res Rep 27:28
9. Wan JG, Wang XW, Wu YJ, Zeng M, Wang Y, Jiang H, Zhou WQ, Wang GH, Liu JM (2005) Appl Phys Lett 86:122501
10. Ding H, Cheah JW, Chen L, Sritharan T, Wang J (2012) Thin Solid Films 522:420
11. Wu YJ, Wan JG, Liu JM, Wang GH (2010) Appl Phys Lett 96:152902
12. Zhao SF, Wu YJ, Wan JG, Dong XW, Liu JM, Wang GH (2008) Appl Phys Lett 92:012920
13. Luo SJ, Wang KF, Li SZ, Dong XW, Yan ZB, Cai HL, Liu JM (2009) Appl Phys Lett 94:172504
14. Yu H, Zeng M, Wang Y, Wan JG, Liu JM (2005) Appl Phys Lett 86:032508
15. Wan JG, Zhang H, Wang XM, Pan DY, Liu JM, Wang GH (2006) Appl Phys Lett 89:122914
16. Murakami M, Chang KS, Aronova MA, Lin CL, Yu MH, Simpers JH, Wuttig M, Takeuchi I, Gao C, Hu B, Lofland SE, Knauss LA, Bendersky LA (2005) Appl Phys Lett 87:112901
17. Zhou JP, He HC, Shi Z, Nan CW (2006) Appl Phys Lett 88:013111
18. Ryu H, Murugavel P, Lee JH, Chae SC, Noh TW, Oh YS, Kim HJ, Kim KH, Jang JH, Kim M, Bae C, Park JG (2006) Appl Phys Lett 89:102907
19. Li JH, Levin I, Slutsker J, Provenzano V, Schenck PK, Ramesh R, Ouyang J, Roytburd AL (2005) Appl Phys Lett 87:072909
20. He HC, Zhou JP, Wang J, Nan CW (2006) Appl Phys Lett 89:052904
21. Zhong XL, Wang JB, Liao M, Huang GJ, Xie SH, Zhou YC, Qiao Y, He JP (2007) Appl Phys Lett 90:152903
22. Zhang N, Srinivasan G, Balbashov AM (2009) J Mater Sci 44:5120
23. Ma J, Hu J, Li Z, Nan CW (2011) Adv Mater 23:1062